EUROPEAN ORGANIZATION FOR NUCLEAR RESEARCH

Elastic differential cross-section measurement at $\sqrt{s} = 13$ TeV by TOTEM

The TOTEM Collaboration

G. Antchev[a], P. Aspell[9], I. Atanassov[a], V. Avati[7], J. Baechler[9], C. Baldenegro Barrera[11], V. Berardi[4a,4b], M. Berretti[2a], E. Bossini[6b], U. Bottigli[6b], M. Bozzo[5a,5b], H. Burkhardt[9], F. S. Cafagna[4a], M. G. Catanesi[4a], M. Csanád[3a,b], T. Csörgő[3a,3b], M. Deile[9], F. De Leonardis[4c,4a], M. Doubek[1c], D. Druzhkin[9], K. Eggert[10], V. Eremin[c], F. Ferro[5a], A. Fiergolski[9], F. Garcia[2a], V. Georgiev[1a], S. Giani[9], L. Grzanka[7], J. Hammerbauer[1a], V. Ivanchenko[8], J. Kašpar[6a,1b], J. Kopal[9], V. Kundrát[1b], S. Lami[6a], G. Latino[6b], R. Lauhakangas[2a], C. Lindsey[11], M. V. Lokajíček[1b], L. Losurdo[6b], M. Lo Vetere[5b,5a,+], F. Lucas Rodríguez[9], M. Macrí[5a], M. Malawski[7], N. Minafra[11], S. Minutoli[5a], T. Naaranoja[2a,2b], F. Nemes[9,3a], H. Niewiadomski[10], T. Novák[3b], E. Oliveri[9], F. Oljemark[2a,2b], M. Oriunno[d], K. Österberg[2a,2b], P. Palazzi[9], V. Passaro[4c,4a], Z. Peroutka[1a], J. Procházka[1c], M. Quinto[4a,4b], E. Radermacher[9], E. Radicioni[4a], F. Ravotti[9], E. Robutti[5a], C. Royon[11], G. Ruggiero[9], H. Saarikko[2a,2b], A. Scribano[6a], J. Smajek[9], W. Snoeys[9], J. Sziklai[3a], C. Taylor[10], E. Tcherniaev[8], N. Turini[6b], V. Vacek[1c], J. Welti[2a,2b], J. Williams[11], R. Ciesielski[12]

[1a]University of West Bohemia, Pilsen, Czech Republic.
[1b]Institute of Physics of the Academy of Sciences of the Czech Republic, Prague, Czech Republic.
[1c]Czech Technical University, Prague, Czech Republic.
[2a]Helsinki Institute of Physics, University of Helsinki, Helsinki, Finland.
[2b]Department of Physics, University of Helsinki, Helsinki, Finland.
[3a]Wigner Research Centre for Physics, RMKI, Budapest, Hungary.
[3b]EKU KRC, Gyöngyös, Hungary.
[4a]INFN Sezione di Bari, Bari, Italy.
[4b]Dipartimento Interateneo di Fisica di Bari, Bari, Italy.
[4c]Dipartimento di Ingegneria Elettrica e dell'Informazione - Politecnico di Bari, Bari, Italy.
[5a]INFN Sezione di Genova, Genova, Italy.
[5b]Università degli Studi di Genova, Italy.
[6a]INFN Sezione di Pisa, Pisa, Italy.
[6b]Università degli Studi di Siena and Gruppo Collegato INFN di Siena, Siena, Italy.
[7]AGH University of Science and Technology, Krakow, Poland.
[8]Tomsk State University, Tomsk, Russia.
[9]CERN, Geneva, Switzerland.
[10]Case Western Reserve University, Dept. of Physics, Cleveland, OH, USA.
[11]The University of Kansas, Lawrence, USA.
[12]Rockefeller Univeristy, New York, USA.

TOTEM collaboration

Abstract

The TOTEM collaboration has measured the elastic proton-proton differential cross section $d\sigma/dt$ at $\sqrt{s} = 13$ TeV LHC energy using dedicated $\beta^* = 90$ m beam optics. The Roman Pot detectors were inserted to 10σ distance from the LHC beam, which allowed the measurement of the range $[0.04\ \text{GeV}^2; 4\ \text{GeV}^2]$ in four-momentum transfer squared $|t|$. The efficient data acquisition allowed to collect about 10^9 elastic events to precisely measure the differential cross-section including the diffractive minimum (dip), the subsequent maximum (bump) and the large-$|t|$ tail. The average nuclear slope has been found to be $B = (20.40 \pm 0.002^{\text{stat}} \pm 0.01^{\text{syst}})$ GeV^{-2} in the $|t|$-range 0.04 GeV^2 to 0.2 GeV^2. The dip position is $|t_{\text{dip}}| = (0.47 \pm 0.004^{\text{stat}} \pm 0.01^{\text{syst}})$ GeV^2. The differential cross section ratio at the bump vs. at the dip $R = 1.77 \pm 0.01^{\text{stat}}$ has been measured with high precision. The series of TOTEM elastic pp measurements show that the dip is a permanent feature of the pp differential cross-section at the TeV scale.

[a]INRNE-BAS, Institute for Nuclear Research and Nuclear Energy, Bulgarian Academy of Sciences, Sofia, Bulgaria.

[b]Department of Atomic Physics, ELTE University, Budapest, Hungary.

[c]Ioffe Physical - Technical Institute of Russian Academy of Sciences, St. Petersburg, Russian Federation.

[d]SLAC National Accelerator Laboratory, Stanford CA, USA.

[+]Deceased.

1 Introduction

This paper presents a high-statistics proton-proton elastic differential cross-section $d\sigma/dt$ measurement by the TOTEM experiment at a center-of-mass LHC energy $\sqrt{s} = 13$ TeV. The square of four-momentum transferred in the elastic process, $|t|$, covers an unprecedented range from 0.04 GeV^2 to 4 GeV^2. The large $|t|$-spectrum has been achieved with special and efficient data acquisition, which allowed to collect an order of 10^9 elastic events. The elastic differential cross-section $d\sigma/dt$ spans ten orders of magnitude in one data set, providing a unique insight into the elastic interaction of protons.

The TOTEM collaboration has already measured proton-proton elastic scattering at several LHC energies: $\sqrt{s} = 2.76$ TeV, 7 TeV, 8 TeV and 13 TeV [1–6]. The present results continue the series of measurements at $\sqrt{s} = 13$ TeV, showing the exponential-like part at low-$|t|$, characterized by an average nuclear slope B, the diffractive minimum of the $d\sigma/dt$ and the perturbative regime.

The main features of the observed $d\sigma/dt$ at the Intersecting Storage Ring (ISR) about 40 years ago are all present at the TeV scale [7]. The $\sqrt{s}$ dependence of the $d\sigma/dt$ shows the shrinkage of the elastic peak with increasing $\sqrt{s}$, thus the average nuclear slope B increases and the dip moves to lower $|t|$ values. The precise data at $\sqrt{s} = 13$ TeV confirms the significant deviation from an exponential in the $|t|$-range from about 0.05 GeV^2 to 0.2 GeV^2, first observed at 8 TeV by the TOTEM experiment [8].

The TOTEM measurements confirmed the existence of the dip at the collision energies $\sqrt{s} = 2.76$ TeV, 7 TeV, 8 TeV and 13 TeV. In total a range of 10 TeV center-of-mass energy is covered, and the observations demonstrate that the diffractive minimum is a permanent structure at the TeV scale [1–6].

2 Experimental setup

The Roman Pot (RP) units used for the present measurement are located on both sides of the LHC Interaction Point 5 (IP5) at distances of ± 213 m (near) and ± 220 m (far), see Fig. 1. A unit consists of 3 RPs, two approaching the outgoing beam vertically and one horizontally. The horizontal RP overlaps with the two verticals and allows for a precise relative alignment of the detectors within the unit. The 7 m long lever arm between the near and the far RP units has the important advantage that the local track angles in the x and y-projections perpendicular to the beam direction can be reconstructed with a precision of about 3 μrad.

Each RP is equipped with a stack of 10 silicon strip detectors designed with the specific objective of reducing the insensitive area at the edge facing the beam to only a few tens of micrometers. The 512 strips with 66 μm pitch of each detector are oriented at an angle of +45° (five planes) and -45° (five planes) with respect to the detector edge [9]. The complete and detailed description of the TOTEM experiment is given in [10, 11].

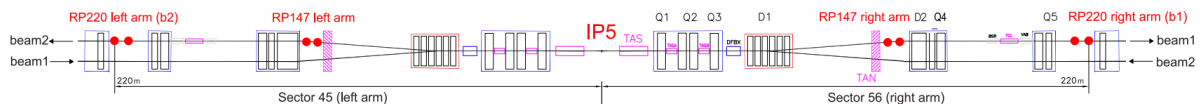**Fig. 1:** (color) Schematic layout of the LHC from IP5 up to the near and far Roman Pot units, where the near and far pots are indicated by full (red) dots on beams 1 and 2.

3 Data taking and analysis

The analysis has been performed on a large data sample, including seven data sets (DS1 - DS7) recorded in 2015, corresponding to the LHC fills 4495, 4496, 4499, 4505, 4509, 4510 and 4511, respectively. The

LHC beam was configured with the $\beta^* = 90$ m optics described in detail in [3, 12–14].

The RP detectors were placed at a distance of 10 times the transverse beam size (σ_{beam}) from the outgoing beams. The special trigger settings allowed to collect about 10^9 elastic events.

The angular resolution is different for each of the data sets DS1-DS7, and it deteriorates with time within the fill, expected mainly due to the beam emittance growth according to $\sigma(x) = \sqrt{\varepsilon\beta}$ [13, 15]. The data sets have been reorganized according to their resolution into two larger data sets. The ones with better(about 20 %) resolution were collected into DS_g, which includes DS1, DS2 and DS4. The remaining ones are collected in data set DS_o. The statistical uncertainties of the scattering angles, obtained from the data, are summarized in Table 2 for the two data sets.

The normalization of this analysis is based on the $\sqrt{s} = 13$ TeV total cross-section measurement with $\beta^* = 90$ m optics, where the RP detectors were placed two times closer ($5\sigma_{\text{beam}}$ distance) to the beam [16]. This data set (DS_n) corresponds to the LHC fill 4489, recorded before DS1.

3.1 Elastic analysis

3.1.1 Reconstruction of kinematics

The horizontal and vertical scattering angles of the proton at IP5 (θ_x^*, θ_y^*) are reconstructed in a given arm by inverting the proton transport equations [14]

$$\theta_x^* = \frac{1}{\frac{dL_x}{ds}}\left(\theta_x - \frac{dv_x}{ds}x^*\right), \, \theta_y^* = \frac{y}{L_y}, \tag{1}$$

where s denotes the distance from the interaction point, y is the vertical coordinate of the proton's trajectory, θ_x is its horizontal angle at the detector, and x^* is the horizontal vertex coordinate reconstructed as

$$x^* = \frac{L_{x,\text{far}} \cdot x_{\text{near}} - L_{x,\text{near}} \cdot x_{\text{far}}}{d}, \tag{2}$$

where $d = (v_{x,\text{near}} \cdot L_{x,\text{far}} - v_{x,\text{far}} \cdot L_{x,\text{near}})$. The scattering angles obtained for the two arms are averaged and the four-momentum transfer squared is calculated as

$$t = -p^2\theta^{*2}, \tag{3}$$

where p is the LHC beam momentum and the scattering angle $\theta^* = \sqrt{\theta_x^{*2} + \theta_y^{*2}}$. Finally, the azimuthal angle is

$$\phi^* = \arctan\left(\frac{\theta_y^*}{\theta_x^*}\right). \tag{4}$$

The coefficients L_x, L_y and v_x of Eq. (1) and Eq. (2) are optical functions of the LHC beam determined by the accelerator magnets between IP5 and the RP detectors, see Fig. 1. The $\beta^* = 90$ m optics is designed with a large vertical effective length $L_y \approx 263$ m at the RPs placed at 220 m from IP5. Since the horizontal effective length L_x is close to zero at the RPs, its derivative $dL_x/ds \approx -0.6$ and the local angle θ_x is used instead. The different reconstruction formula in the vertical and horizontal plane in Eq. (1) is also motivated by their different sensitivity to LHC magnet and beam perturbations.

3.1.2 RP alignment and beam optics

After applying the usual TOTEM alignment methods the residual misalignment is about 3.3 μm in the horizontal coordinate and about 110 μm in the vertical. When propagated to the reconstructed scattering angles, this leads to uncertainties about 1.11 μrad (horizontal angle) and 0.42 μrad (vertical angle) [2, 8].

Table 1: The physics analysis cuts and their characteristic width σ for DS_g in Diagonal 1 (the other diagonal agrees within the quoted uncertainty). The width σ of the horizontal and vertical collinearity cuts define the resolution in the scattering angle, see Fig. 2.

	Name		σ
1	Vertical collinearity cut	[μrad]	1.87 ± 0.01
2	Spectrometer cut, left arm	[μm]	15.9 ± 0.3
3	Spectrometer cut, right arm	[μm]	14.6 ± 0.3
4	Horizontal vertex cut	[μm]	7.3 ± 1.0
5	Horizontal collinearity cut	[μrad]	4.96 ± 0.02

The nominal optics has been updated from LHC magnet and current databases and calibrated using the observed elastic candidates of DS_n. The calibrated optics has been used in the analysis of DS_g and DS_o exploiting the stability of the LHC optics. The uncertainties of the optical functions have been estimated with a Monte Carlo program applying the optics calibration procedure on a sophisticated simulation of the LHC beam and its perturbations. The obtained uncertainty is about 1.2 ‰ for dL_x/ds and 2.1 ‰ for L_y [13, 14].

3.1.3 Event selection

The analysis is similar to the procedure performed for the measurement of the elastic cross section at several other LHC energies [1–6]. The measurement of the elastic events is based on the selection of events with the following topology in the RP detector system: a reconstructed track in the near and far vertical detectors on each side of the IP such that the elastic signature is satisfied in one of the two diagonals: left bottom and right top (Diagonal 1) or left top and right bottom (Diagonal 2).
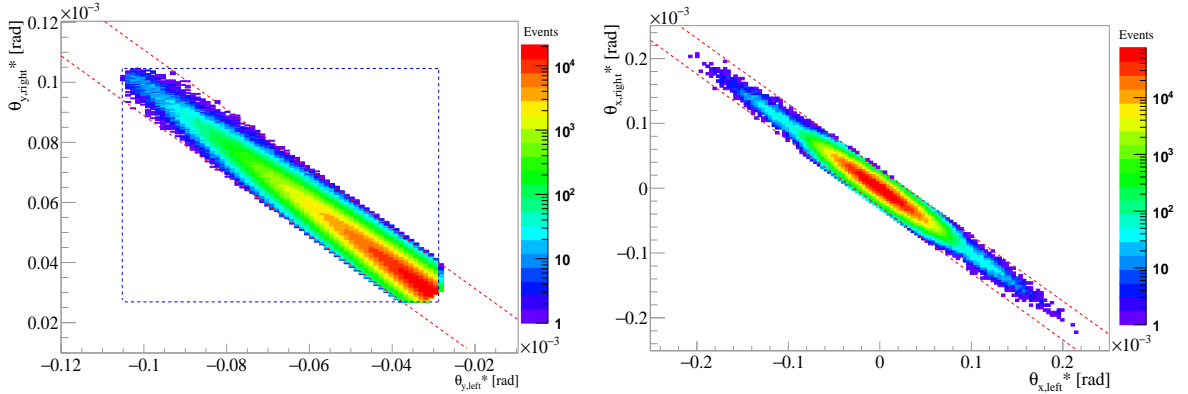

Fig. 2: (color) The collinearity of the vertical and horizontal scattering angles. The blue lines represent the angular acceptance cuts in the vertical plane around the acceptance edges. The red ones show the 4σ physics cuts to require the collinarity of the angles in both projections.

In addition, the elastic event selection requires the collinearity of the outgoing protons in the two arms, see Fig. 2. The suppression of the diffractive events is also required using the correlation between the position y and the inclination $\Delta y = y_{far} - y_{near}$ with so-called spectrometer cuts, see Table 1. The equality of the horizontal vertex position x^* reconstructed from the left and right arms is also required.

Fig. 2 shows the horizontal collinearity cut imposing momentum conservation in the horizontal plane with 1 ‰ uncertainty. The cuts are applied at the 4σ level, and they are optimized for purity (background contamination in the selected sample less than 0.1 %) and for efficiency (uncertainty of true elastic event selection 0.5 %). Fig. 3 shows the progressive selection of elastic events after each analysis cut following the order in Table 1.
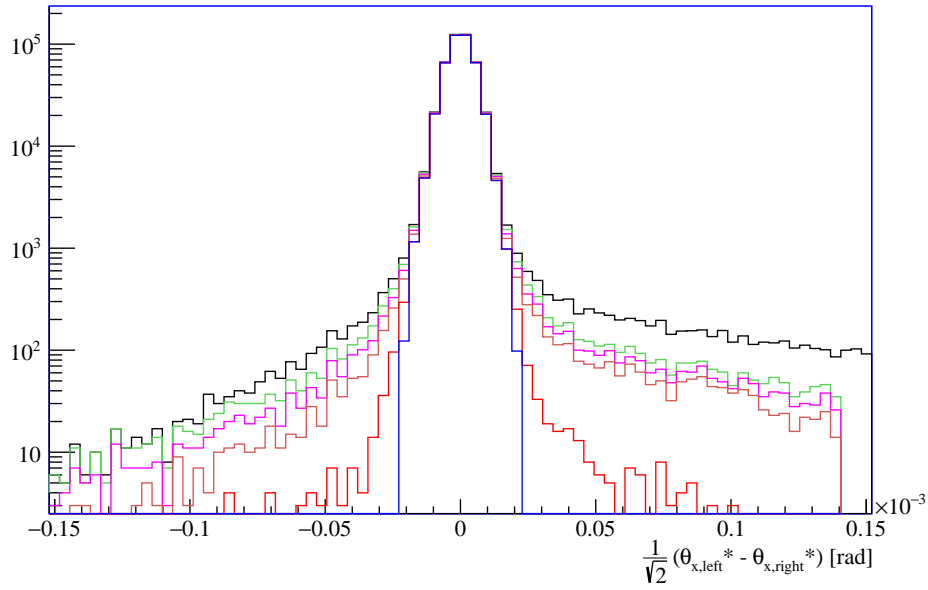
Fig. 3: (color) The horizontal beam divergence estimated from the data of Diagonal 1 by comparing the reconstructed horizontal scattering angle θ_x^* of the left and right arm. The distribution is shown before any analysis cut (black solid line) and after each analysis cut following the order in Table 1.

3.1.4 Geometrical and beam divergence correction, unfolding
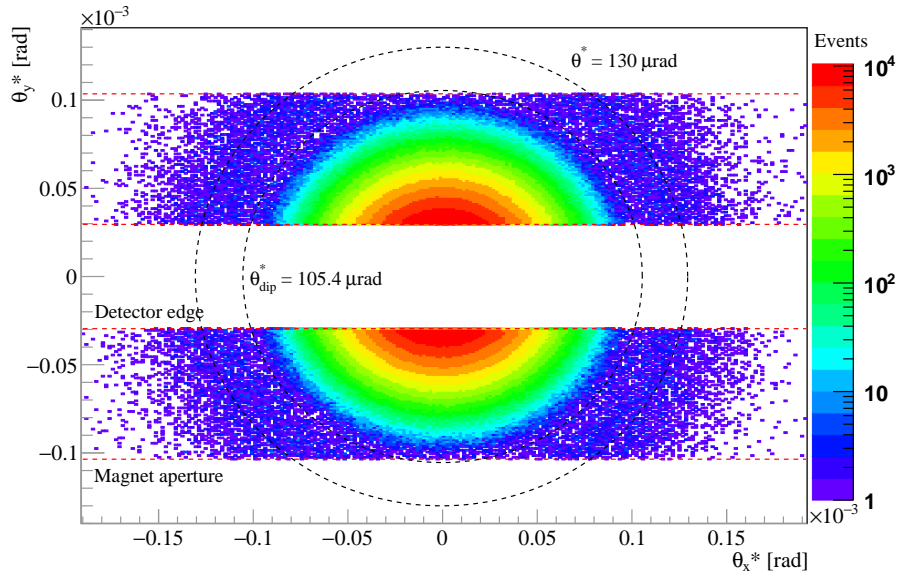
Fig. 4: (color) The azimuthal distribution of the scattering angle θ^* demonstrates the azimuthal symmetry of elastic scattering on a data sample from Diagonal 1 and 2. The red dashed lines show the analysis acceptance cuts, which define the acceptance boundaries near the detector edge and magnet aperture. The inner black dashed circle illustrates the approximate scattering angle position θ_{dip}^* of the diffractive minimum in the data.

The acceptance of elastically scattered protons is limited by the RP silicon detector edge and by the LHC magnet apertures. The acceptance boundaries are defined by the acceptance cuts shown in Fig. 4. Fig. 4 also shows the $|t|$-acceptance circle for the range of the diffractive minimum at $\theta_{\mathrm{dip}}^* = 105.4\,\mu\mathrm{rad}$.

Fig. 5: (color) The geometrical acceptance correction $\mathcal{A}(t)$ is defined by the cuts of Fig. 4. The beam divergence correction $D(t_y)$ depends on the vertical collinearity cut θ_y^* shown in Fig 2: the angular window and the σ of the cut determines the missing acceptance in the corners. Note that the data extends up to 4.0 GeV^2 due to the horizontal acceptance, see also Fig. 2.
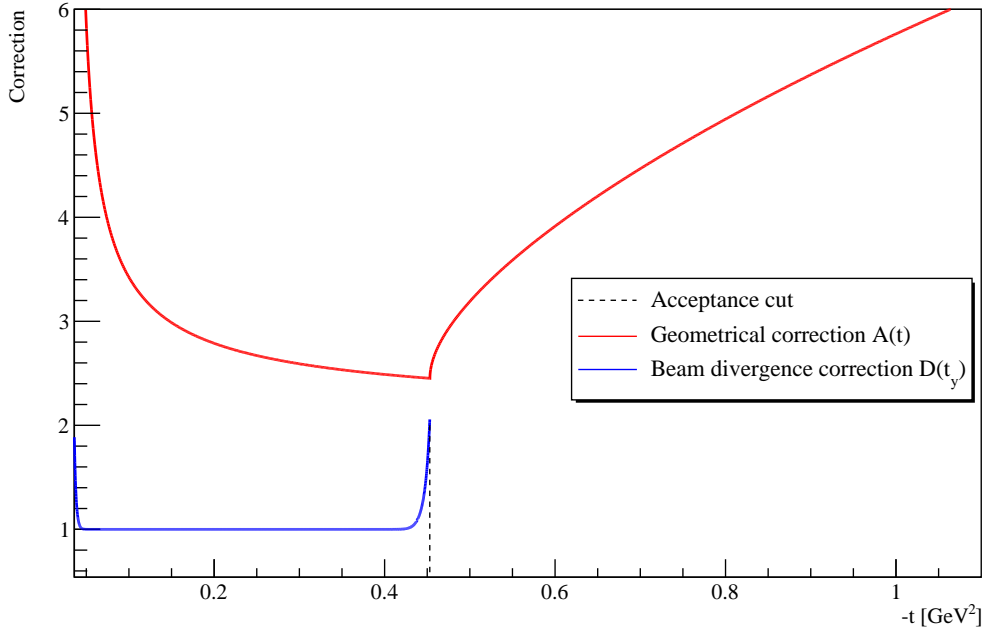
The geometrical acceptance correction is calculated in order to correct for the missing acceptance in ϕ^*

$$\mathcal{A}(t) = \frac{2\pi}{\Delta\phi^*(t)}, \tag{5}$$

where $\Delta\phi^*$ is the visible azimuthal angle range.

The correction function $\mathcal{A}(t)$ is drawn as a solid red line in Fig. 5. The function is monotonically decreasing between the detector edge cut at $|t|_{y,\min} = 0.04$ GeV^2 and the aperture cut at $|t|_{y,\max} = 0.45$ GeV^2, since in this range the visible ϕ part of the acceptance circles is increasing with $|t|$. At the largest $|t|$-values of the analysis, about 4 GeV ^{2}, the maximum of the correction function $\mathcal{A}(t)$ is about 13.

The acceptance cut at the acceptance edges is not step function-like due to the angular spread, the beam divergence, of the LHC beam. The effect of the beam divergence can be directly measured by comparing the angles reconstructed from the left and right arm, see Fig. 2. The figure shows the correlation between the angles and at the same time the spread due to the beam divergence. The figure also shows the missing corners of the acceptance at the acceptance edges. This additional acceptance loss is modeled with a Gaussian distribution, with experimentally determined parameters. The beam divergence correction $\mathcal{D}(t_y)$ is drawn as a solid blue line in Fig. 5, which is close to 1 except at the acceptance edges.

Finally, the acceptance correction $\mathcal{A}(t)\mathcal{D}(t_y)$ is factorized in terms of the geometrical and beam divergence corrections.

The unfolding of resolution effects has been estimated with a Monte Carlo simulation whose parameters are obtained from the data, see Table 2. The probability distribution $p(t)$ of the event generator is based on the fit of the differential rate dN/dt. Each generated MC event is propagated to the RP detectors with the proper model of the LHC optics, which takes into account the beam divergence and other resolution effects. The kinematics of the event is reconstructed and a histogram is built from the four momentum transfer squared t values. The ratio of the histograms without and with resolution effect describes the

Table 2: Horizontal and vertical angular resolutions of the analysis data sets DS_g and DS_o, respectively.

	Horizontal	Vertical
	[μrad]	
DS_g	4.96 ± 0.02	1.87 ± 0.01
DS_o	5.10 ± 0.02	2.24 ± 0.01
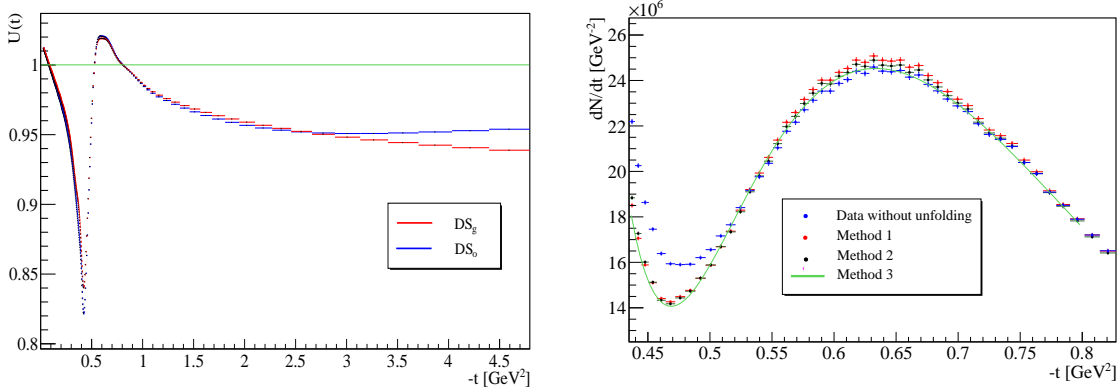
Fig. 6: (color) The unfolding correction histograms $U(t)$ for data set DS_g and DS_o, which correspond to the resolution values summarized in Table 2 (left panel). Comparison of the unfolding of dN_{el}/dt using the three unfolding methods around the diffractive minimum (right panel).

first approximation of the bin-by-bin corrections due to bin migration. The probability distribution $p(t)$ of the simulation is multiplied with the correction histogram, to modulate the source, and the procedure is repeated until the histogram with migration effects coincides with the measured distribution, thus the correct source distribution has been found. The uncertainty of the unfolding procedure is estimated from the residual difference between the measured histogram dN_{el}/dt and the simulated histogram with resolution effects.

According to Table 2 the angular resolution is different in the horizontal and vertical plane, so the simulation takes into account the angular acceptance cuts of the analysis to give the proper weight to the resolution effects. The angular spread of the beam is determined with an uncertainty of 0.1 μrad by comparing the scattering angles reconstructed from the left and right arm, therefore the unfolding correction factor $\mathcal{U}(t)$ can be calculated with a precision better than 0.1 %. The unfolding correction histograms $U(t)$ are shown in Fig. 6. Three different unfolding methods have been compared in order to estimate the contribution of the unfolding to the systematic uncertainty: the described MC based algorithm (Method 1), regularized unfolding (Method 2) and deconvolution of a proper fit function with resolution σ (Method 3) [17]. The results of the three methods are perfectly consistent within their uncertainties, see Fig. 6.

In total, the event-by-event correction factor due to acceptance corrections and resolution unfolding is

$$\mathcal{C}(t,t_y) = \mathcal{A}(t)\mathcal{D}(t_y)\mathcal{U}(t). \tag{6}$$

3.1.5 Inefficiency corrections

The proton reconstruction efficiency of the RP detectors is evaluated directly from the data. The RP detectors are unable to resolve multiple tracks, which is the main source of detector inefficiency [10]. The additional tracks can be due to interactions of the protons with the sensors or the surrounding material, or due to pileup with non-signal protons or beam halo.

Table 3: Corrections to the differential rate for the two diagonals. The "uncorrelated" inefficiency correction ($\mathcal{I}_{3/4}$) is t-dependent, in the table the average correction on the elastic rate is provided.

Correction	Diagonal 1	Diagonal 2
$\mathcal{I}_{3/4}$ [%]	11.2 ± 1.1	12.25 ± 1.4

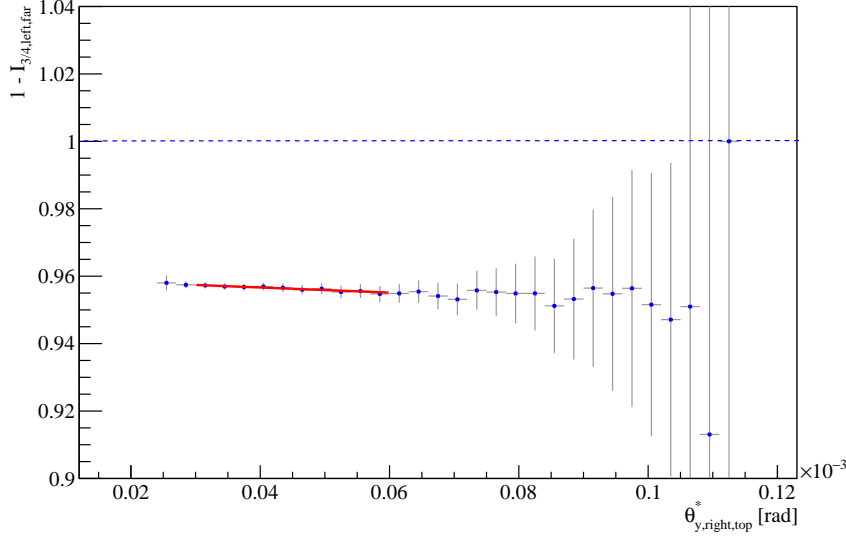**Fig. 7:** (color) The contribution of the left far pot to the $\mathcal{I}_{3/4}$ correction in Diagonal 1. The inefficiency as a function of θ_y^* is estimated with a linear fit, shown with a solid red line.

The inefficiency corrections are calculated for different categories: "uncorrelated" ($\mathcal{I}_{3/4}$), when one RP out of four along a diagonal has no reconstructed track; this inefficiency includes the loss of the elastic proton due to an additional track coming from nuclear interaction, shower or pile-up with a beam halo proton. The $\mathcal{I}_{3/4}$ inefficiency has been determined using a reduced set of elastic cuts in a so-called "3/4" elastic analysis per detector and diagonal [8]. The inefficiency is determined as a function of θ_y^* per RP, see Fig. 7, which shows that the dependence on the angle is close to negligible. The overall correction on the elastic rate is described in Table 3.

The inefficiency is called "correlated" ($\mathcal{I}_{2/4}$) when both RP of one arm have no reconstructed tracks. The case when the inefficient RPs are in different arms is denoted with $\mathcal{I}_{2/4\,\mathrm{diff.}}$. The present analysis focuses on the differential cross-section measurement, and its overall normalization is determined from the corresponding cross section analysis at 13 TeV [16]. The t-dependence of the inefficiencies $\mathcal{I}_{2/4}$ and $\mathcal{I}_{2/4\,\mathrm{diff.}}$ is even weaker than for $\mathcal{I}_{3/4}$, thus these inefficiencies are estimated but set to zero in the total correction factor per event (shown in its most general form)

$$f(t,t_y) = \frac{1}{\eta_\mathrm{d}\eta_\mathrm{tr}} \cdot \frac{\mathcal{C}(t,t_y)}{1-\mathcal{I}} \cdot \frac{1}{\Delta t}, \tag{7}$$

where the track reconstruction inefficiency $\mathcal{I} = \mathcal{I}_{3/4}(\theta_y^*) + \mathcal{I}_{2/4} + \mathcal{I}_{2/4\,\mathrm{diff}} = \mathcal{I}_{3/4}(\theta_y^*)$ and Δt is the bin width. The η_d, η_tr are the DAQ and trigger efficiencies that influence the normalization only. However, during the final normalization to the total cross-section these parameters cancel [16].

4 The differential cross section

After inefficiency correction the differential rates $\mathrm{d}N/\mathrm{d}t$ of the two diagonals (Diagonal 1 and 2) agree within their statistical uncertainty. The two diagonals are almost independent measurements, thus the

final measured differential rate is calculated as the bin-by-bin weighted average of the two differential elastic rates dN_{el}/dt, according to their systematic uncertainty.

The normalization is based on the 13 TeV total cross-section measurement with $\beta^* = 90$ m optics, where the RP detectors were placed at half the distance to the beam ($5\sigma_{beam}$ instead of 10σ distance) [16]. The ρ measurement at 13 TeV with $\beta^* = 2500$ m optics was also essential to obtain the final normalization [18]. The differential cross-section is shown in Fig. 8. The normalization uncertainty 5.5 % is determined by the total cross-section measurement, inheriting the normalization uncertainty from [16].

The numerical values of the differential cross-section, the representative $|t|$-values, as well as the statistical and systematic uncertainties are given in Tables 5-10.
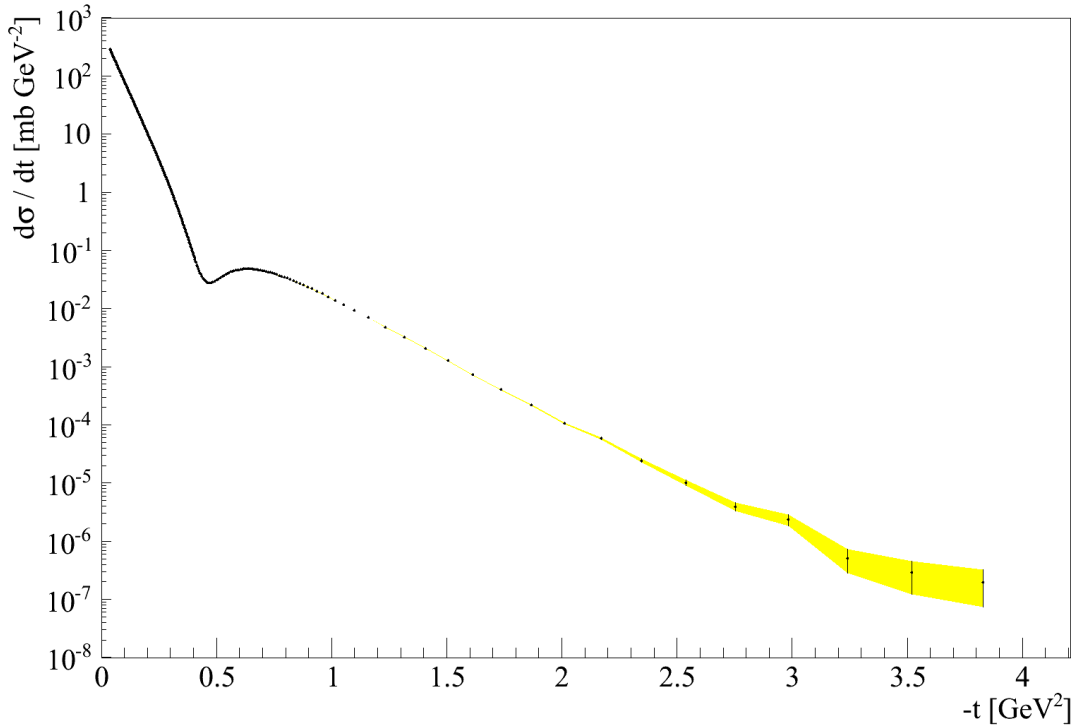
Fig. 8: (color) Differential elastic cross-section $d\sigma/dt$ at $\sqrt{s} = 13$ TeV. The statistical and $|t|$-dependent correlated systematic uncertainty envelope is shown as a yellow band.

The propagation of systematic uncertainties to the $|t|$-distribution has been estimated with a Monte Carlo program, see Fig. 9. A fit of the final differential cross-section data is used to generate the true reference $|t|$-distribution. Simultaneously, another $|t|$-distribution is created, which is perturbed with one of the systematic effects at 1σ level. The difference between the $|t|$-distributions gives the systematic effect on the differential cross-section

$$\delta s_q(t) \equiv \frac{\partial (d\sigma/dt)}{\partial q} \delta q, \tag{8}$$

where δq corresponds to 1σ bias in the quantity q responsible for a given systematic effect. The Monte-Carlo simulations show that the combined effect of several systematic errors is well approximated by linear combination of the individual contributions from Eq. (8).
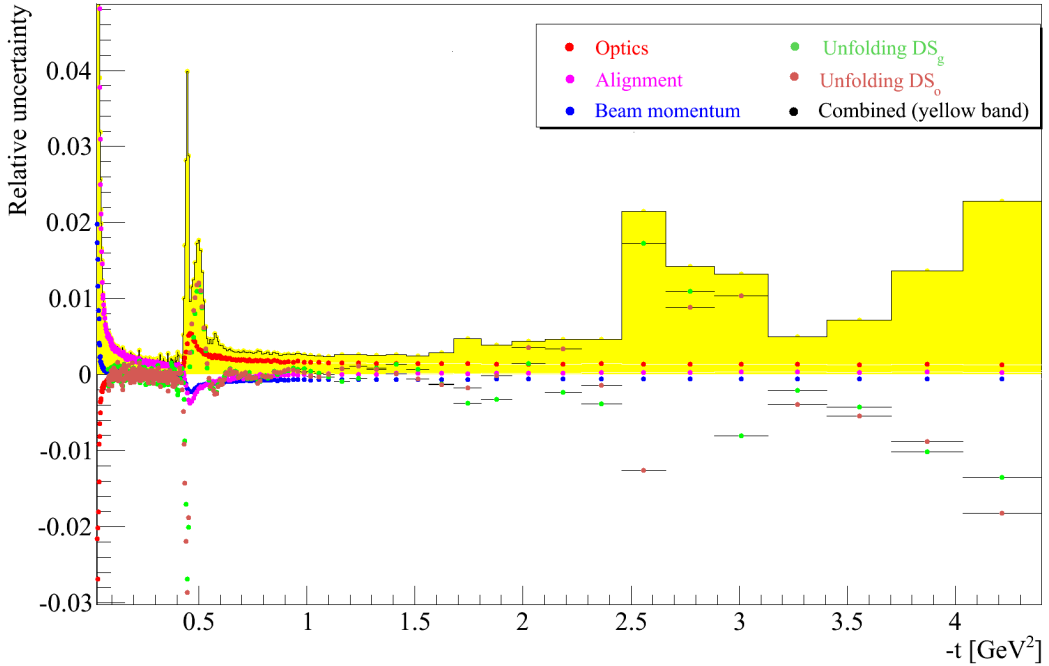
Fig. 9: (color) Summary of the $|t|$-dependent systematic uncertainties. The figure shows the systematic uncertainties due to 1σ optics, alignment and beam momentum perturbations. The contribution of the unfolding into the systematic uncertainty is also presented. The yellow band is the combined systematics uncertainty.

The $|t|$-dependent systematic uncertainties are summarized in Fig. (9). The result can be used to approximate the covariance matrix of systematic uncertainties:

$$V_{ij} = \sum_q \delta s_q(i) \delta s_q(j),$$

(9)

where i and j are bin indices, and the sum over q goes over the optics, alignment and beam momentum error contributions. The model fits of the data have been evaluated using the covariance matrix in the generalized least-squares method

$$\chi^2 = \Delta^T V^{-1} \Delta, \quad \Delta_i = \left(\frac{d\sigma}{dt} - f(t)|_{t=t_\text{repr}} \right)_{\text{bin } i}$$

(10)

and $V = V_\text{stat} + V_\text{syst}$.

The nuclear slope has been found to be $B = (20.40 \pm 0.002^\text{stat} \pm 0.01^\text{syst})$ GeV^{-2} using an exponential fit in the $|t|$-range from 0.04 GeV^2 to 0.2 GeV^2. The relative difference between data and this fit is plotted in Fig. 10, showing a non-exponential shape, similar to the 8 TeV result [8]. Consequently, the value found for the nuclear slope B can be considered as an average B and the fit quality $\chi^2/\text{ndf} = 1175.3/92$ shows that the exponential model is an oversimplified description of the data. To obtain a better fit one can generalize the pure exponential to a cumulant expansion:

$$\frac{d\sigma}{dt}(t) = \frac{d\sigma}{dt}\bigg|_{t=0} \exp\left(\sum_{i=1}^{N_b} b_i t^i \right),$$

(11)

where the $N_b = 1$ case corresponds to the exponential. The $N_b = 3$ case is the first which provides a satisfactory description of the data, with $\chi^2/\text{ndf} = 109.5/90$ and p-value=8.0 %, see Fig. 10.
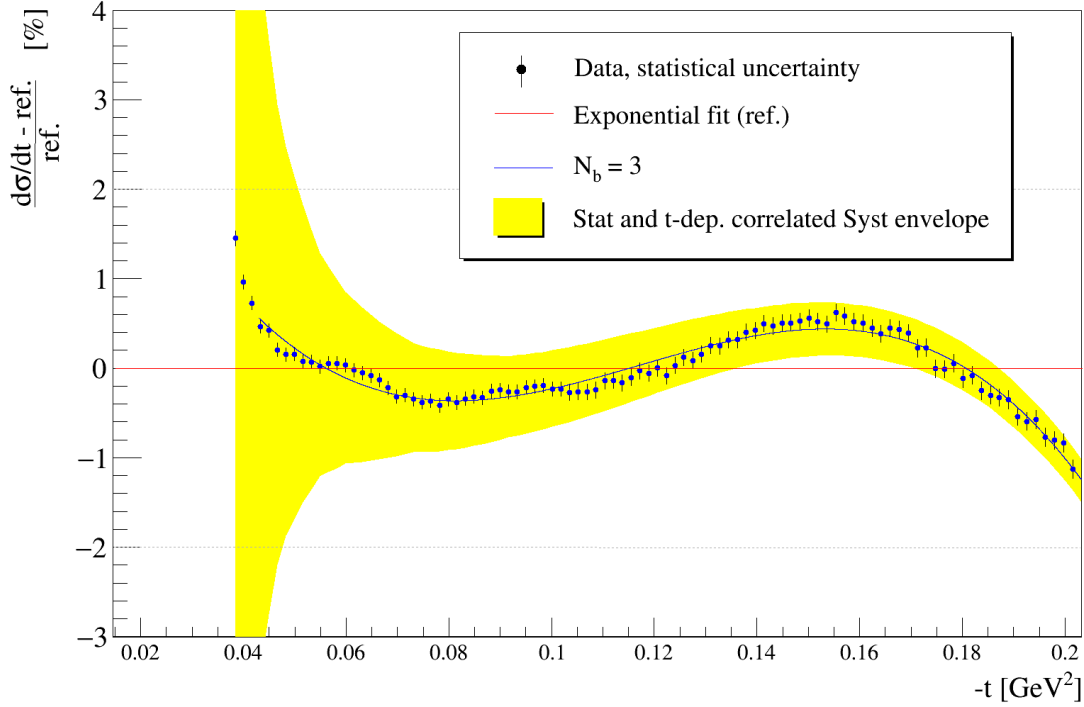
Fig. 10: The non-exponential part of the data. The statistical and $|t|$-dependent correlated systematic uncertainty envelope is shown as a yellow band, while the data points show the statistical uncertainty.

The diffractive minimum and the subsequent maximum has been observed with great accuracy, see Fig. 11. The dip position has been found to be $|t_{\text{dip}}| = (0.47 \pm 0.004^{\text{stat}} \pm 0.01^{\text{syst}})$ GeV^2. The statistical uncertainty is the half the bin width, while the systematic is determined by the combined $|t|$-resolution of the two diagonals. The ratio of the differential cross-section values at the diffractive minimum and at the subsequent maximum has been found to be $R = 1.77 \pm 0.01$. The value of R is calculated from the value of the maximum and minimum bin, since the data is very precise and the bin-by-bin fluctuations are on the 5 ‰ level. The uncertainty is calculated from the statistical uncertainty of the two bins, since the systematic uncertainty of the dip and bump follows the same pattern, hence the systematic uncertainty of R is negligible.

The large-$|t|$ part of the measured differential cross section, starting from $t = 2.1$ GeV^2 up to 4 GeV^2, is consistent with a power law behavior (p-value=80 %). The fitted exponent is of the order of 10, compatible with lower energy measurements [7], and high energy predictions [19].

Table 4: The main physics observables and their statistical and systematic uncertainty.

Physics quantity	Value	Total uncertainty Stat. $\oplus$ Syst.
B [GeV^{-2}]	20.40	$0.002 \oplus 0.01 = 0.01$
$|t_{\text{dip}}|$ [GeV^2]	0.47	$0.004 \oplus 0.01 = 0.01$
R	1.77	0.01

5 Summary

The TOTEM collaboration has measured the elastic proton-proton differential cross section $d\sigma/dt$ at $\sqrt{s} = 13$ TeV LHC energy in the four-momentum transfer squared $|t|$ range from 0.04 GeV^2 to 4 GeV^2.
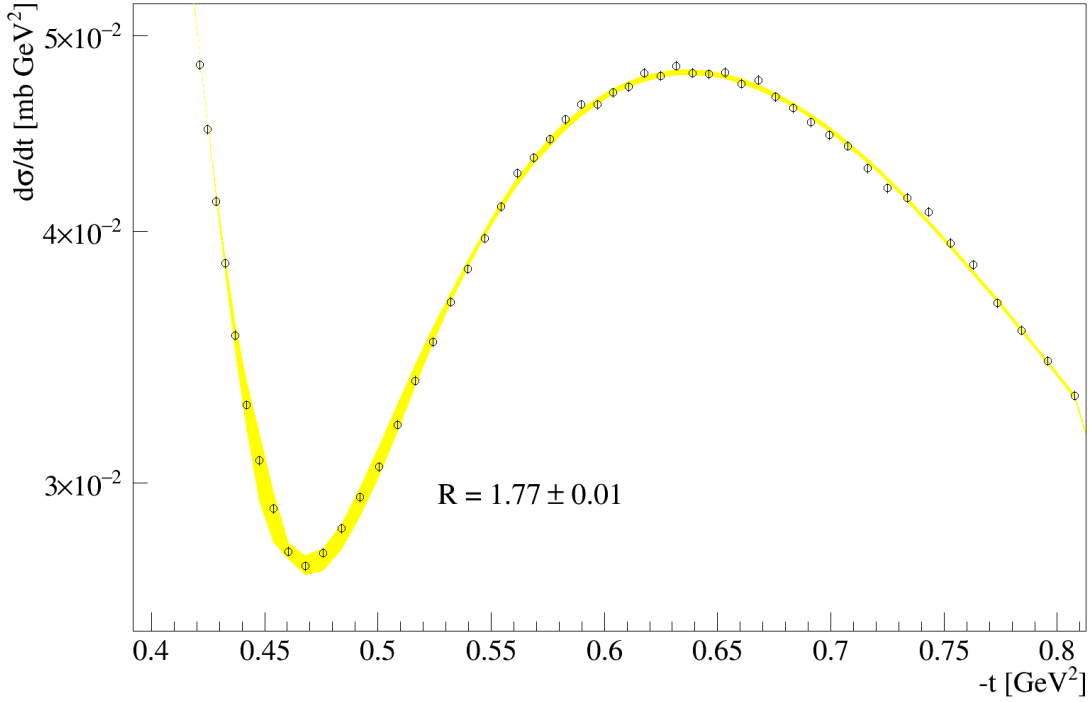
Fig. 11: The diffractive minimum has been observed with high significance at 13 TeV. The uncertainty on the points is the statistical uncertainty, while the yellow band shows the full uncertainty, including the systematic part. The dip position has been found to be $|t_{\mathrm{dip}}| = (0.47 \pm 0.004^{\mathrm{stat}} \pm 0.01^{\mathrm{syst}})$ GeV^2 and the differential cross section ratio between the second maximum and the minimum is $R = 1.77 \pm 0.01^{\mathrm{stat}}$.

The special data acquisition allowed to collect about 10^9 elastic events and the precise measurement of the differential cross-section including, the diffractive minimum and the large-$|t|$ tail. The average nuclear slope has been found to be $B = (20.40 \pm 0.002^{\mathrm{stat}} \pm 0.01^{\mathrm{syst}})$ GeV^{-2} in the $|t|$-range 0.04 GeV^2 to 0.2 GeV^2. The position of the diffractive minimum is $|t_{\mathrm{dip}}| = (0.47 \pm 0.004^{\mathrm{stat}} \pm 0.01^{\mathrm{syst}})$ GeV^2 and the differential cross section ratio at the maximum and minimum is $R = 1.77 \pm 0.01^{\mathrm{stat}}$ with negligible systematic uncertainty.

Acknowledgments

Table 5: The differential cross-section $\mathrm{d}\sigma/\mathrm{d}t$

$|t|_{\text{low}}$	$|t|_{\text{high}}$ [GeV^2]	$|t|_{\text{repr.}}$	$\mathrm{d}\sigma/\mathrm{d}t$	Statistical uncertainty [mb GeV^{-2}]	Systematic uncertainty
0.03763	0.03926	0.03840	291.005	0.238	23.23
0.03926	0.04090	0.04004	280.102	0.219	17.10
0.04090	0.04254	0.04168	270.253	0.208	13.45
0.04254	0.04419	0.04332	260.682	0.198	10.17
0.04419	0.04583	0.04496	251.980	0.191	8.04
0.04583	0.04748	0.04661	243.144	0.183	6.23
0.04748	0.04912	0.04825	234.997	0.177	5.10
0.04912	0.05077	0.04990	227.243	0.171	4.35
0.05077	0.05242	0.05155	219.549	0.165	3.65
0.05242	0.05408	0.05320	212.265	0.159	3.08
0.05408	0.05573	0.05486	205.123	0.154	2.55
0.05573	0.05739	0.05651	198.390	0.149	2.27
0.05739	0.05904	0.05817	191.804	0.144	2.01
0.05904	0.06070	0.05983	185.387	0.139	1.77
0.06070	0.06236	0.06149	179.122	0.135	1.63
0.06236	0.06402	0.06315	173.102	0.130	1.49
0.06402	0.06569	0.06481	167.281	0.126	1.36
0.06569	0.06735	0.06648	161.621	0.122	1.24
0.06735	0.06902	0.06814	156.083	0.118	1.13
0.06902	0.07069	0.06981	150.719	0.114	1.03
0.07069	0.07236	0.07148	145.698	0.110	0.94
0.07236	0.07403	0.07315	140.756	0.107	0.85
0.07403	0.07571	0.07482	135.985	0.103	0.81
0.07571	0.07738	0.07650	131.443	0.100	0.76
0.07738	0.07906	0.07818	126.963	0.097	0.72
0.07906	0.08074	0.07985	122.778	0.094	0.67
0.08074	0.08242	0.08153	118.598	0.091	0.63
0.08242	0.08410	0.08322	114.650	0.088	0.60
0.08410	0.08579	0.08490	110.811	0.085	0.56
0.08579	0.08747	0.08658	107.055	0.082	0.53
0.08747	0.08916	0.08827	103.514	0.080	0.49
0.08916	0.09085	0.08996	100.023	0.077	0.46
0.09085	0.09254	0.09165	96.617	0.075	0.43
0.09254	0.09423	0.09334	93.343	0.072	0.41
0.09423	0.09593	0.09503	90.220	0.070	0.39
0.09593	0.09762	0.09673	87.164	0.068	0.38
0.09762	0.09932	0.09842	84.210	0.066	0.36
0.09932	0.10102	0.10012	81.310	0.064	0.34
0.10102	0.10272	0.10182	78.544	0.062	0.33
0.10272	0.10442	0.10353	75.835	0.069	0.31
0.10442	0.10613	0.10523	73.253	0.067	0.30
0.10613	0.10783	0.10693	70.749	0.064	0.28
0.10783	0.10954	0.10864	68.344	0.062	0.27
0.10954	0.11125	0.11035	66.073	0.060	0.26
0.11125	0.11296	0.11206	63.812	0.058	0.24
0.11296	0.11468	0.11377	61.604	0.056	0.23
0.11468	0.11639	0.11549	59.525	0.054	0.22
0.11639	0.11811	0.11720	57.524	0.052	0.21
0.11811	0.11983	0.11892	55.529	0.050	0.20
0.11983	0.12154	0.12064	53.648	0.049	0.19
0.12154	0.12327	0.12236	51.755	0.047	0.18
0.12327	0.12499	0.12408	50.026	0.045	0.17
0.12499	0.12671	0.12580	48.342	0.044	0.16
0.12671	0.12844	0.12753	46.655	0.042	0.16

Table 6: Continuation of Table 5.

$|t|_{\text{low}}$	$|t|_{\text{high}}$ [GeV^2]	$|t|_{\text{repr.}}$	dσ/dt	Statistical uncertainty [mb GeV^{-2}]	Systematic uncertainty
0.12844	0.13017	0.12926	45.0718	0.0409	0.148
0.13017	0.13190	0.13099	43.5530	0.0396	0.141
0.13190	0.13363	0.13272	42.0412	0.0383	0.134
0.13363	0.13537	0.13445	40.6083	0.0370	0.127
0.13537	0.13710	0.13618	39.1987	0.0357	0.120
0.13710	0.13884	0.13792	37.8674	0.0346	0.114
0.13884	0.14058	0.13966	36.5563	0.0334	0.108
0.14058	0.14232	0.14140	35.3093	0.0323	0.104
0.14232	0.14406	0.14314	34.0693	0.0312	0.099
0.14406	0.14580	0.14488	32.8900	0.0302	0.095
0.14580	0.14755	0.14663	31.7420	0.0292	0.091
0.14755	0.14930	0.14837	30.6370	0.0282	0.088
0.14930	0.15105	0.15012	29.5747	0.0273	0.084
0.15105	0.15280	0.15187	28.5268	0.0264	0.080
0.15280	0.15455	0.15363	27.5185	0.0256	0.077
0.15455	0.15630	0.15538	26.5863	0.0247	0.074
0.15630	0.15806	0.15713	25.6414	0.0239	0.071
0.15806	0.15982	0.15889	24.7246	0.0231	0.068
0.15982	0.16158	0.16065	23.8487	0.0224	0.065
0.16158	0.16334	0.16241	22.9954	0.0216	0.062
0.16334	0.16510	0.16417	22.1702	0.0209	0.059
0.16510	0.16687	0.16594	21.4001	0.0203	0.057
0.16687	0.16864	0.16770	20.6409	0.0196	0.054
0.16864	0.17040	0.16947	19.9019	0.0190	0.052
0.17040	0.17218	0.17124	19.1646	0.0183	0.050
0.17218	0.17395	0.17301	18.4862	0.0177	0.048
0.17395	0.17572	0.17478	17.7879	0.0172	0.045
0.17572	0.17750	0.17656	17.1552	0.0166	0.043
0.17750	0.17927	0.17834	16.5560	0.0161	0.042
0.17927	0.18105	0.18011	15.9388	0.0155	0.040
0.18105	0.18283	0.18189	15.3767	0.0151	0.038
0.18283	0.18462	0.18368	14.8025	0.0146	0.036
0.18462	0.18640	0.18546	14.2666	0.0141	0.035
0.18640	0.18819	0.18725	13.7533	0.0137	0.033
0.18819	0.18998	0.18903	13.2581	0.0132	0.032
0.18998	0.19177	0.19082	12.7590	0.0128	0.030
0.19177	0.19356	0.19261	12.2949	0.0124	0.029
0.19356	0.19535	0.19440	11.8561	0.0120	0.028
0.19535	0.19715	0.19620	11.4076	0.0116	0.026
0.19715	0.19894	0.19800	10.9936	0.0113	0.025
0.19894	0.20074	0.19979	10.5950	0.0109	0.024
0.20074	0.20254	0.20159	10.1833	0.0106	0.023
0.20254	0.20435	0.20339	9.8035	0.0102	0.022
0.20435	0.20615	0.20520	9.4488	0.0099	0.021
0.20615	0.20796	0.20700	9.1026	0.0096	0.020
0.20796	0.20977	0.20881	8.7620	0.0093	0.019
0.20977	0.21158	0.21062	8.4083	0.0090	0.018
0.21158	0.21339	0.21243	8.1080	0.0087	0.017
0.21339	0.21520	0.21424	7.8116	0.0084	0.016
0.21520	0.21702	0.21606	7.5264	0.0082	0.016
0.21702	0.21883	0.21787	7.2372	0.0079	0.015
0.21883	0.22065	0.21969	6.9655	0.0077	0.014
0.22065	0.22247	0.22151	6.7154	0.0075	0.013
0.22247	0.22429	0.22333	6.4637	0.0072	0.013

Table 7: Continuation of Table 5.

$|t|_{\text{low}}$	$|t|_{\text{high}}$	$|t|_{\text{repr.}}$	$d\sigma/dt$	Statistical uncertainty	Systematic uncertainty
	[GeV^2]			[mb GeV^{-2}]	
0.22429	0.22612	0.22515	6.20908	0.0070	0.0122
0.22612	0.22794	0.22698	5.97031	0.0068	0.0116
0.22794	0.22977	0.22881	5.75469	0.0066	0.0111
0.22977	0.23160	0.23064	5.53763	0.0064	0.0105
0.23160	0.23343	0.23247	5.32432	0.0062	0.0101
0.23343	0.23527	0.23430	5.11779	0.0060	0.0097
0.23527	0.23710	0.23613	4.91989	0.0058	0.0093
0.23710	0.23894	0.23797	4.72926	0.0057	0.0089
0.23894	0.24078	0.23981	4.54239	0.0055	0.0085
0.24078	0.24262	0.24165	4.37635	0.0053	0.0081
0.24262	0.24446	0.24349	4.20548	0.0052	0.0078
0.24446	0.24631	0.24533	4.03536	0.0050	0.0075
0.24631	0.24815	0.24718	3.89381	0.0049	0.0071
0.24815	0.25000	0.24902	3.73005	0.0047	0.0068
0.25000	0.25185	0.25087	3.58604	0.0046	0.0065
0.25185	0.25370	0.25272	3.44067	0.0044	0.0062
0.25370	0.25556	0.25458	3.30493	0.0043	0.0060
0.25556	0.25741	0.25643	3.17651	0.0042	0.0057
0.25741	0.25927	0.25829	3.04288	0.0040	0.0055
0.25927	0.26113	0.26015	2.92947	0.0039	0.0052
0.26113	0.26299	0.26201	2.80257	0.0038	0.0050
0.26299	0.26485	0.26387	2.69417	0.0037	0.0048
0.26485	0.26672	0.26573	2.57945	0.0036	0.0046
0.26672	0.26858	0.26760	2.47640	0.0035	0.0044
0.26858	0.27045	0.26947	2.37881	0.0034	0.0042
0.27045	0.27232	0.27134	2.27509	0.0033	0.0040
0.27232	0.27420	0.27321	2.18539	0.0032	0.0038
0.27420	0.27607	0.27508	2.09632	0.0031	0.0036
0.27607	0.27795	0.27695	2.00623	0.0030	0.0035
0.27795	0.27982	0.27883	1.92209	0.0029	0.0033
0.27982	0.28170	0.28071	1.84416	0.0028	0.0031
0.28170	0.28359	0.28259	1.76460	0.0027	0.0030
0.28359	0.28547	0.28447	1.69359	0.0027	0.0029
0.28547	0.28735	0.28636	1.62036	0.0026	0.0027
0.28735	0.28924	0.28824	1.54873	0.0025	0.0026
0.28924	0.29113	0.29013	1.48620	0.0024	0.0025
0.29113	0.29302	0.29202	1.42084	0.0024	0.0024
0.29302	0.29492	0.29391	1.35815	0.0023	0.0022
0.29492	0.29681	0.29581	1.29937	0.0022	0.0021
0.29681	0.29871	0.29770	1.24334	0.0022	0.0020
0.29871	0.30061	0.29960	1.18712	0.0021	0.0019
0.30061	0.30251	0.30150	1.13726	0.0021	0.0018
0.30251	0.30441	0.30340	1.08606	0.0020	0.0018
0.30441	0.30631	0.30531	1.03785	0.0019	0.0017
0.30631	0.30822	0.30721	0.99128	0.0019	0.0016
0.30822	0.31013	0.30912	0.94404	0.0018	0.0015
0.31013	0.31204	0.31103	0.90267	0.0018	0.0014
0.31204	0.31395	0.31294	0.86103	0.0017	0.0014
0.31395	0.31586	0.31485	0.82014	0.0017	0.0013
0.31586	0.31778	0.31677	0.78056	0.0016	0.0012
0.31778	0.31970	0.31868	0.74955	0.0016	0.0012
0.31970	0.32162	0.32060	0.71498	0.0015	0.0011
0.32162	0.32354	0.32252	0.67820	0.0015	0.0010
0.32354	0.32546	0.32445	0.64830	0.0014	0.0010

Table 8: Continuation of Table 5.

$\|t\|_{\text{low}}$	$\|t\|_{\text{high}}$ [GeV^2]	$\|t\|_{\text{repr.}}$	$\mathrm{d}\sigma/\mathrm{d}t$	Statistical uncertainty [mb GeV^{-2}]	Systematic uncertainty
0.32546	0.32739	0.32637	0.6160172	0.00140	0.00094
0.32739	0.32932	0.32830	0.5875874	0.00136	0.00090
0.32932	0.33124	0.33022	0.5599290	0.00132	0.00086
0.33124	0.33318	0.33215	0.5326184	0.00129	0.00081
0.33318	0.33511	0.33409	0.5084319	0.00125	0.00077
0.33511	0.33704	0.33602	0.4841120	0.00121	0.00074
0.33704	0.33898	0.33796	0.4584498	0.00118	0.00070
0.33898	0.34092	0.33989	0.4368558	0.00114	0.00067
0.34092	0.34286	0.34183	0.4159908	0.00111	0.00063
0.34286	0.34480	0.34378	0.3931062	0.00108	0.00060
0.34480	0.34675	0.34572	0.3773297	0.00105	0.00057
0.34675	0.34870	0.34767	0.3567071	0.00102	0.00054
0.34870	0.35064	0.34961	0.3408495	0.00099	0.00052
0.35064	0.35259	0.35156	0.3233294	0.00096	0.00049
0.35259	0.35455	0.35351	0.3078857	0.00093	0.00047
0.35455	0.35650	0.35547	0.2911156	0.00090	0.00044
0.35650	0.35846	0.35742	0.2759747	0.00088	0.00042
0.35846	0.36042	0.35938	0.2632198	0.00085	0.00040
0.36042	0.36238	0.36134	0.2484736	0.00083	0.00038
0.36238	0.36434	0.36330	0.2368378	0.00080	0.00036
0.36434	0.36630	0.36526	0.2238501	0.00078	0.00035
0.36630	0.36827	0.36723	0.2129791	0.00076	0.00034
0.36827	0.37024	0.36920	0.2001638	0.00073	0.00032
0.37024	0.37221	0.37117	0.1910685	0.00071	0.00031
0.37221	0.37418	0.37314	0.1811450	0.00069	0.00030
0.37418	0.37616	0.37511	0.1708701	0.00067	0.00029
0.37616	0.37813	0.37709	0.1631546	0.00065	0.00028
0.37813	0.38011	0.37906	0.1542701	0.00063	0.00027
0.38011	0.38209	0.38104	0.1458654	0.00061	0.00025
0.38209	0.38407	0.38302	0.1376252	0.00059	0.00024
0.38407	0.38606	0.38501	0.1314138	0.00058	0.00023
0.38606	0.38804	0.38699	0.1250128	0.00056	0.00022
0.38804	0.39003	0.38898	0.1172248	0.00054	0.00020
0.39003	0.39202	0.39097	0.1108358	0.00053	0.00019
0.39202	0.39401	0.39296	0.1051992	0.00051	0.00018
0.39401	0.39601	0.39495	0.0988553	0.00049	0.00017
0.39601	0.39800	0.39695	0.0943577	0.00048	0.00016
0.39800	0.40000	0.39894	0.0893882	0.00047	0.00014
0.40000	0.40200	0.40094	0.0844118	0.00045	0.00013
0.40200	0.40410	0.40299	0.0794673	0.00043	0.00012
0.40410	0.40631	0.40514	0.0746659	0.00040	0.00011
0.40631	0.40866	0.40742	0.0702312	0.00038	0.00010
0.40866	0.41117	0.40984	0.0644914	0.00035	0.00008
0.41117	0.41384	0.41242	0.0612570	0.00033	0.00008
0.41384	0.41668	0.41517	0.0562343	0.00030	0.00008
0.41668	0.41974	0.41812	0.0526126	0.00028	0.00007
0.41974	0.42305	0.42129	0.0483678	0.00026	0.00007
0.42305	0.42663	0.42473	0.0449274	0.00024	0.00011
0.42663	0.43054	0.42846	0.0413754	0.00022	0.00022
0.43054	0.43483	0.43255	0.0385490	0.00020	0.00038
0.43483	0.43957	0.43705	0.0354994	0.00019	0.00061
0.43957	0.44485	0.44204	0.0327863	0.00017	0.00093
0.44485	0.45072	0.44760	0.0307740	0.00016	0.00122
0.45072	0.45722	0.45377	0.0291248	0.00015	0.00084

Table 9: Continuation of Table 5.

$|t|_{\text{low}}$	$|t|_{\text{high}}$ [GeV^2]	$|t|_{\text{repr.}}$	dσ/dt	Statistical uncertainty [mb GeV^{-2}]	Systematic uncertainty
0.45722	0.46437	0.46059	0.0277333	0.00015	0.00027
0.46437	0.47203	0.46799	0.0272682	0.00014	0.00032
0.47203	0.48006	0.47585	0.0276871	0.00015	0.00035
0.48006	0.48828	0.48398	0.0284679	0.00015	0.00042
0.48828	0.49654	0.49222	0.0294984	0.00015	0.00051
0.49654	0.50472	0.50045	0.0305493	0.00016	0.00054
0.50472	0.51278	0.50857	0.0320606	0.00017	0.00053
0.51278	0.52069	0.51656	0.0337122	0.00018	0.00045
0.52069	0.52845	0.52440	0.0352345	0.00019	0.00034
0.52845	0.53607	0.53209	0.0368763	0.00020	0.00024
0.53607	0.54356	0.53964	0.0382915	0.00020	0.00018
0.54356	0.55093	0.54707	0.0396758	0.00021	0.00019
0.55093	0.55820	0.55440	0.0411312	0.00022	0.00019
0.55820	0.56539	0.56163	0.0427254	0.00022	0.00021
0.56539	0.57250	0.56878	0.0434895	0.00023	0.00022
0.57250	0.57956	0.57587	0.0444147	0.00023	0.00024
0.57956	0.58657	0.58290	0.0454339	0.00024	0.00022
0.58657	0.59356	0.58990	0.0462303	0.00024	0.00020
0.59356	0.60052	0.59687	0.0462224	0.00024	0.00019
0.60052	0.60748	0.60383	0.0468683	0.00025	0.00018
0.60748	0.61444	0.61079	0.0471657	0.00025	0.00017
0.61444	0.62142	0.61776	0.0479109	0.00025	0.00017
0.62142	0.62844	0.62476	0.0477659	0.00025	0.00016
0.62844	0.63550	0.63179	0.0483139	0.00025	0.00016
0.63550	0.64262	0.63888	0.0479224	0.00025	0.00016
0.64262	0.64981	0.64603	0.0478640	0.00025	0.00015
0.64981	0.65710	0.65327	0.0479463	0.00025	0.00015
0.65710	0.66449	0.66060	0.0473400	0.00025	0.00015
0.66449	0.67200	0.66805	0.0475291	0.00025	0.00014
0.67200	0.67966	0.67563	0.0466393	0.00025	0.00014
0.67966	0.68747	0.68336	0.0460401	0.00024	0.00014
0.68747	0.69545	0.69125	0.0452852	0.00024	0.00014
0.69545	0.70363	0.69933	0.0446399	0.00024	0.00013
0.70363	0.71203	0.70761	0.0440867	0.00023	0.00013
0.71203	0.72066	0.71611	0.0429611	0.00023	0.00013
0.72066	0.72956	0.72487	0.0419997	0.00022	0.00012
0.72956	0.73875	0.73391	0.0415542	0.00022	0.00012
0.73875	0.74826	0.74324	0.0408855	0.00021	0.00012
0.74826	0.75812	0.75292	0.0394498	0.00021	0.00011
0.75812	0.76837	0.76296	0.0384823	0.00020	0.00011
0.76837	0.77905	0.77341	0.0368327	0.00019	0.00011
0.77905	0.79021	0.78432	0.0357022	0.00019	0.00010
0.79021	0.80190	0.79572	0.0344881	0.00018	0.00010
0.80190	0.81419	0.80769	0.0331379	0.00017	0.00009
0.81419	0.82715	0.82029	0.0317622	0.00017	0.00009
0.82715	0.84087	0.83361	0.0301535	0.00016	0.00008
0.84087	0.85546	0.84773	0.0286175	0.00015	0.00008
0.85546	0.87105	0.86279	0.0268686	0.00014	0.00007
0.87105	0.88781	0.87892	0.0257198	0.00013	0.00007
0.88781	0.90598	0.89633	0.0236250	0.00012	0.00006
0.90598	0.92585	0.91528	0.0217698	0.00012	0.00006
0.92585	0.94787	0.93614	0.0199802	0.00011	0.00005
0.94787	0.97267	0.95942	0.0179976	0.00010	0.00005
0.97267	1.00119	0.98591	0.0159908	0.00008	0.00004

Table 10: Continuation of Table 5.

$|t|_{\text{low}}$	$|t|_{\text{high}}$	$|t|_{\text{repr.}}$	$\mathrm{d}\sigma/\mathrm{d}t$	Statistical uncertainty	Systematic uncertainty
	[GeV^2]			[mb GeV^{-2}]	
1.00119	1.03483	1.01673	0.01377598	0.00007261	0.000036737
1.03483	1.07580	1.05364	0.01160554	0.00006101	0.000030768
1.07580	1.12787	1.09948	0.00933244	0.00004911	0.000024537
1.12787	1.19956	1.15991	0.00700284	0.00003679	0.000018286
1.19956	1.27842	1.23455	0.00478260	0.00002953	0.000012760
1.27842	1.36517	1.31661	0.00323285	0.00002357	0.000008191
1.36517	1.46060	1.40681	0.00206329	0.00001825	0.000005511
1.46060	1.56556	1.50598	0.00125878	0.00001387	0.000003100
1.56556	1.68102	1.61503	0.00072459	0.00001022	0.000002075
1.68102	1.80803	1.73499	0.00040267	0.00000740	0.000001886
1.80803	1.94774	1.86706	0.00021747	0.00000530	0.000000856
1.94774	2.10142	2.01215	0.00010673	0.00000360	0.000000473
2.10142	2.27047	2.17127	0.00005870	0.00000260	0.000000276
2.27047	2.45642	2.34561	0.00002434	0.00000163	0.000000114
2.45642	2.66097	2.53863	0.00001017	0.00000102	0.000000215
2.66097	2.88597	2.75357	0.00000395	0.00000063	0.000000055
2.88597	3.13348	2.98393	0.00000235	0.00000050	0.000000031
3.13348	3.40573	3.23982	0.00000051	0.00000023	0.000000003
3.40573	3.70521	3.52028	0.00000029	0.00000017	0.000000002
3.70521	4.03464	3.82873	0.00000020	0.00000012	0.000000003

References

[1] G. Antchev *et al.* (TOTEM collaboration), *Phys. Rev. Lett.* **111** (2013) .

[2] G. Antchev *et al.* (TOTEM collaboration), *Eur. Phys. J.* **C76** (2016) .

[3] G. Antchev *et al.* (TOTEM collaboration), *EPL* **96** (2011) .

[4] G. Antchev *et al.* (TOTEM collaboration), *EPL* **101** (2013) .

[5] F. Nemes, *PoS (DIS2017) 059* (2017) .

[6] G. Antchev *et al.* (TOTEM collaboration), in preparation: *Measurement of proton-proton elastic scattering and total cross-section at $\sqrt{s}$= 2.76 TeV* (2018) .

[7] U. Amaldi and K. R. Schubert *Nucl. Phys.* **B166** (1980) 301–320.

[8] G. Antchev *et al.* (TOTEM collaboration), *Nucl. Phys.* **B899** (2015) 527–546.

[9] G. Ruggiero *et al. Nucl. Instrum. Meth.* **A604** (2009) 242–245.

[10] G. Anelli *et al.* (TOTEM collaboration), *JINST* **3** (2008) S08007.

[11] G. Antchev *et al.* (TOTEM collaboration), *TOTEM Upgrade Proposal* (2013) . http://cds.cern.ch/record/1554299.

[12] G. Antchev *et al.* (TOTEM collaboration), *EPL* **101** (2013) .

[13] F. Nemes, *Elastic scattering of protons at the TOTEM experiment at the LHC*. PhD thesis, Eötvös U., CERN-THESIS-2015-293, 2015.

[14] G. Antchev *et al.* (TOTEM collaboration), *New J. Phys.* **16** (2014) 103041.

[15] H. Niewiadomski, *Reconstruction of protons in the TOTEM roman pot detectors at the LHC*. PhD thesis, Manchester U., 2008. http://weblib.cern.ch/abstract?CERN-THESIS-2008-080.

[16] G. Antchev *et al.* (TOTEM collaboration), *CERN-EP-2017-321* (2017) . http://cds.cern.ch/record/2296409.

[17] G. Cowan, *Statistical data analysis*. 1998.

[18] G. Antchev *et al.* (TOTEM collaboration), *CERN-EP-2017-335* (2017) . https://cds.cern.ch/record/2298154.

[19] S. J. Brodsky and G. R. Farrar *Phys. Rev. Lett.* **31** (1973) 1153–1156.